Chapter

Exploring Associative Learning of Audio and Color Stimuli with Neuromorphic Robots in a T-Maze

Md Abu Bakr Siddique, Tianze Liu, Yan Zhang and Hongyu An

Abstract

Deep neural networks (DNNs) have achieved remarkable success in various cognitive tasks through training on extensive labeled datasets. However, the heavy reliance on these datasets poses challenges for DNNs in scenarios with energy constraints in particular scenarios, such as on the moon. On the contrary, animals exhibit a self-learning capability by interacting with their surroundings and memorizing concurrent events without annotated data—a process known as associative learning. A classic example of associative learning is when a rat memorizes desired and undesired stimuli while exploring a T-maze. The successful implementation of associative learning aims to replicate the self-learning mechanisms observed in animals, addressing challenges in data-constrained environments. While current implementations of associative learning are predominantly small scale and offline, this work pioneers associative learning in a robot equipped with a neuromorphic chip, specifically for online learning in a T-maze. The system successfully replicates classic associative learning observed in rodents, using neuromorphic robots as substitutes for rodents. The neuromorphic robot autonomously learns the cause-and-effect relationship between audio and visual stimuli.

Keywords: associative learning, Hebbian learning, neuromorphic computing, neuromorphic robot, neuromorphic chip

1. Introduction

Deep neural networks (DNNs) have demonstrated remarkable success across various cognitive tasks [1], primarily attributed to their training on extensive datasets. DNNs refine their accuracy during training by comparing predictions against labeled data and adjusting their weights through backpropagation algorithms. Generally, larger datasets and more intricate neural networks yield superior accuracy [1, 2], leading to a continual push for larger datasets and more complex architectures [1–5]. However, the increasing size of DNNs and dependence on labeled datasets bring significant challenges, including high power consumption, data scarcity, and limited flexibility in autonomous operations. These challenges render DNNs less ideal for applications with stringent size, weight, and power (SWaP) constraints [1, 2], such as planetary rovers that demand high adaptability and autonomy with minimal human oversight in energy-limited and communication-restricted environments [2].

To mitigate these issues, we aim to enhance the autonomous capabilities of intelligent robots by mimicking animal associative learning through neuromorphic systems. These systems provide a more energy-efficient approach to artificial intelligence by replicating brain functions. Associative learning, a prevalent self-learning mechanism in animals, allows them to adapt to their environment by remembering concurrent events through interaction [6–8]. A quintessential example of this learning process is seen in rodents navigating a T-maze, where they learn to associate specific stimuli with positive or negative outcomes through repeated exposures. For instance, one arm of the maze might lead to a reward like food, while the other might offer no reward or a mild aversive stimulus. This associative learning process can similarly empower robots to link information and experiences, enabling them to autonomously navigate and adapt in dynamic environments, such as those encountered on Mars.

Several studies have investigated associative learning [7, 9–15] but often face limitations such as small-scale neural networks, a preference for simulations over real-world experiments, and a lack of real-world robotic deployment for testing [11–15]. To address these limitations, we have taken a novel approach. We developed a large-scale associative learning system using a neuromorphic chip (the Xylo chip) and deployed it on a mobile robot for online learning through real-world interactions. This successful implementation of associative learning in a real-world robotic deployment reassures the practicality of our research. The robot, mimicking rodents in a T-maze, learns by associating audio and visual signals as conditional and unconditional stimuli.

Our research marks a significant advancement in artificial intelligence and robotics. By implementing classical T-maze associative learning on a mobile robot in real-world settings, we have not only enhanced our understanding of associative learning but also paved the way for developing more efficient and adaptable robots. The integration of the Xylo chip with mobile robots has notably improved their signal processing speed and energy efficiency, making them more viable for practical applications. This work inspires us to imagine a future where robots can navigate and adapt in dynamic environments, such as those encountered on Mars, with minimal human intervention. The improved signal processing speed and energy efficiency of robots integrated with the Xylo chip should make us all feel optimistic about the future of robotics.

In our experiments, the red color input is an unconditional and aversive stimulus, while audio signals function as conditional and neutral stimuli. The neuromorphic robot learns to avoid the arm presenting the red color in the T-maze, with distinct neural assemblies processing the color and auditory signals.

This chapter's contributions are as follows:

1. Replicating the classical rodent associative learning paradigm in a T-maze in real time, both in simulations and experimental settings.

2. Implementing a neural assembly designed as a decision-making component and applying it to the associative learning paradigm in the T-maze.

2. Background of rodents' associative learning in T-maze

The T-maze paradigm is a pivotal tool in the study of associative learning in rodents, particularly rats, which holds significant importance. It offers profound insights into spatial navigation and memory processes. The experimental setup, featuring a T-shaped maze with distinct arms and a decision point, presents a unique challenge to the rats, compelling them to navigate and make choices based on spatial cues.

Initially, rats display exploratory behavior, moving through the maze without a specific preference for either arm. As the experiments progress, their behavior changes markedly. Through repeated trials, the rats begin to form associations between particular stimuli or cues in the arms and the outcomes of their choices. This learning process becomes evident as the rats consistently favor one arm, driven by the expectation of a positive reward, such as food.

The adaptability of rats in T-maze experiments is a testament to the dynamic nature of associative learning. These rodents demonstrate remarkable cognitive flexibility, adjusting their arm choices in response to changing spatial cues or new stimuli. For instance, when the location of the reward is altered, rats undergo a learning phase to realign their choices with the new reward location, showcasing their ability to adapt to new contingencies.

The neural mechanisms driving associative learning in the T-maze are intricate and complex, involving a web of interactions within the rat's brain. Key brain regions involved in memory, spatial navigation, and reward processing play crucial roles. The T-maze paradigm serves as an invaluable tool for delving into the fundamental principles of cognitive processes and behavior in mammals, casting light on the underlying neural circuitry and its adaptability.

3. Associative learning with neuromorphic robots

Our associative learning system, with its two distinct signal pathways for processing auditory and visual inputs, as illustrated in **Figure 1**, has the potential to revolutionize the field. This configuration empowers the neuromorphic robot to handle auditory and visual stimuli simultaneously, thereby greatly improving its learning efficiency.

The auditory pathway is a key component of our system, which captures and decodes sound cues and enables the robot to interpret and learn from auditory signals in its environment. Meanwhile, the visual pathway processes visual data and allows the robot to identify and respond to visual stimuli essential for associative learning. Integrating these pathways enriches the robot's cognitive abilities, facilitating a deeper understanding of the cause-and-effect relationships between auditory and visual inputs.

3.1 Audio and visual perception using a neuromorphic system

Figure 2(a) depicts the architecture of the audio perception neural network. Auditory data is imported into 16 channels via a microphone, aligning with the capabilities of the Xylo chip, as shown in **Figure 2(b)**. For this study, we focused on a

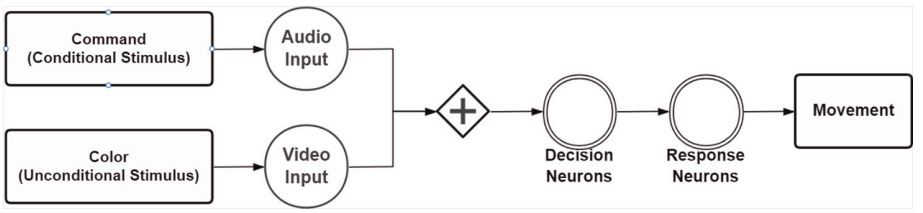

Figure 1.
Overall associative learning implementation.

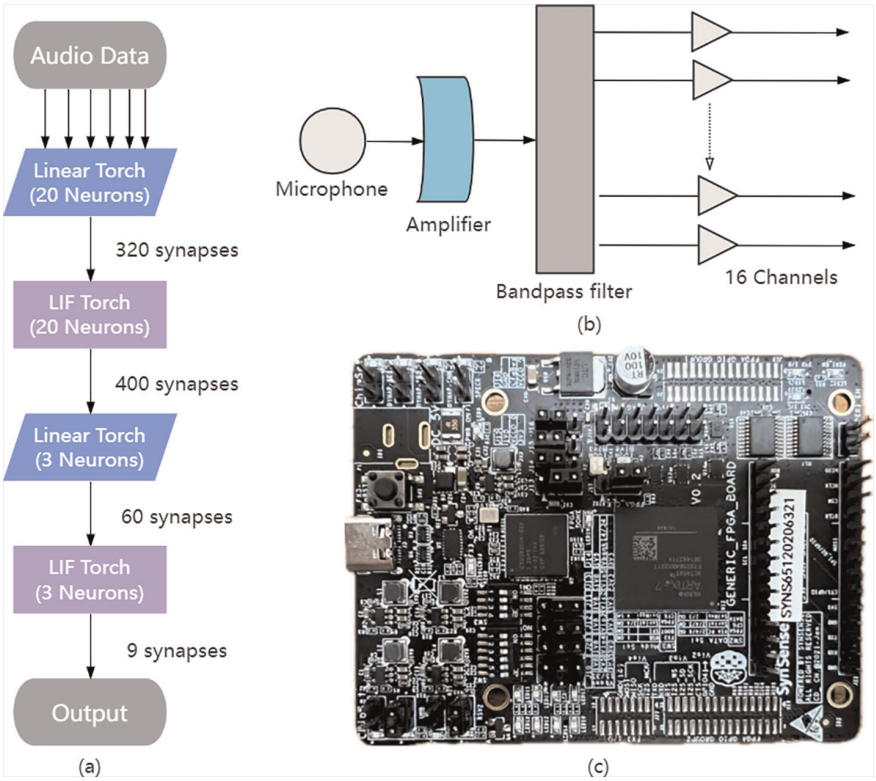

Figure 2.
(a) Audio perception neural network architecture. (b) Preprocessing module of Xylo neuromorphic chip. (c) XyloA2TestBoard for audio command detector model deployment.

subset of commands, specifically "left" and "right". The auditory data was reorganized by transforming events into frames. **Figure 2(c)** illustrates the Xylo neuromorphic chip processing audio perception.

The network architecture consists of an input layer with 16 channels, processed through a hidden layer containing 20 neurons. The final output layer produces 3 units. The simulations operate with a timestep of 10 milliseconds.

The input data was structured into tensors to seamlessly integrate with our model, enabling the generation of visual representations for the "left" and "right" audio commands. **Figures 3** and **4** illustrate the spiking signals for the "left" and "right" commands processed by the Xylo neuromorphic chips. The spiking neural networks (SNNs) underwent training for 17,500 epochs. Utilizing the Adam optimizer with a learning rate 1e-5, the model achieved a 92.

3.2 Power usage of Xylo neuromorphic chip

During the deployment of our trained SNNs on the Xylo neuromorphic chip, power consumption emerged as a crucial metric for assessing the system's efficiency in processing "left" and "right" audio commands. **Table 1** shows that the Logic component is the highest power consumer, drawing 1844.26 mW. The IO circuitry and the analog front-end (AFE) IO components consume 213.94 and 230.98 mW, respectively. Importantly, the Logic AFE component has high efficiency and

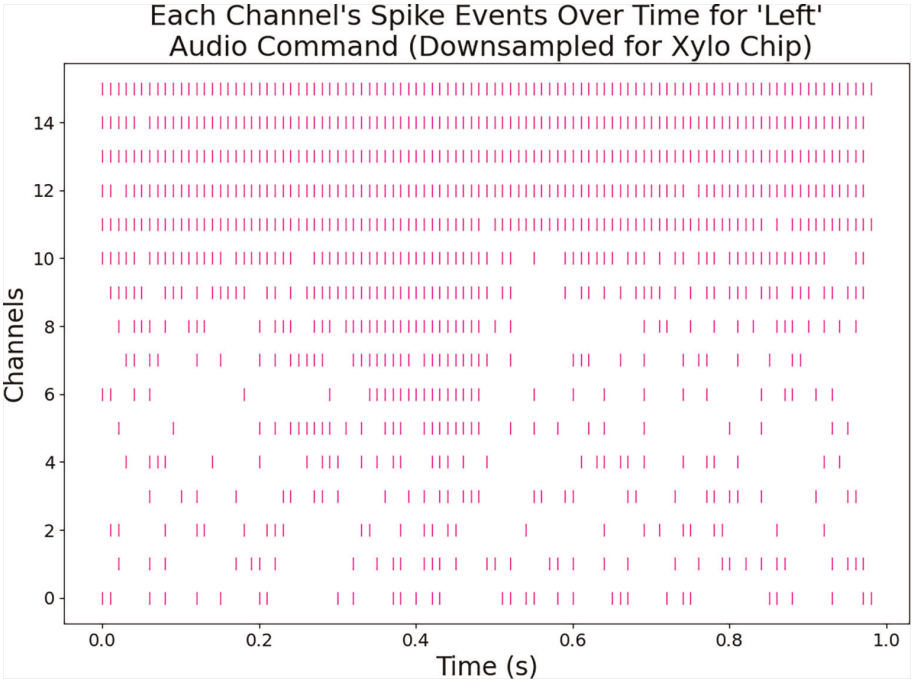

Figure 3.
Spike events for a left audio command.

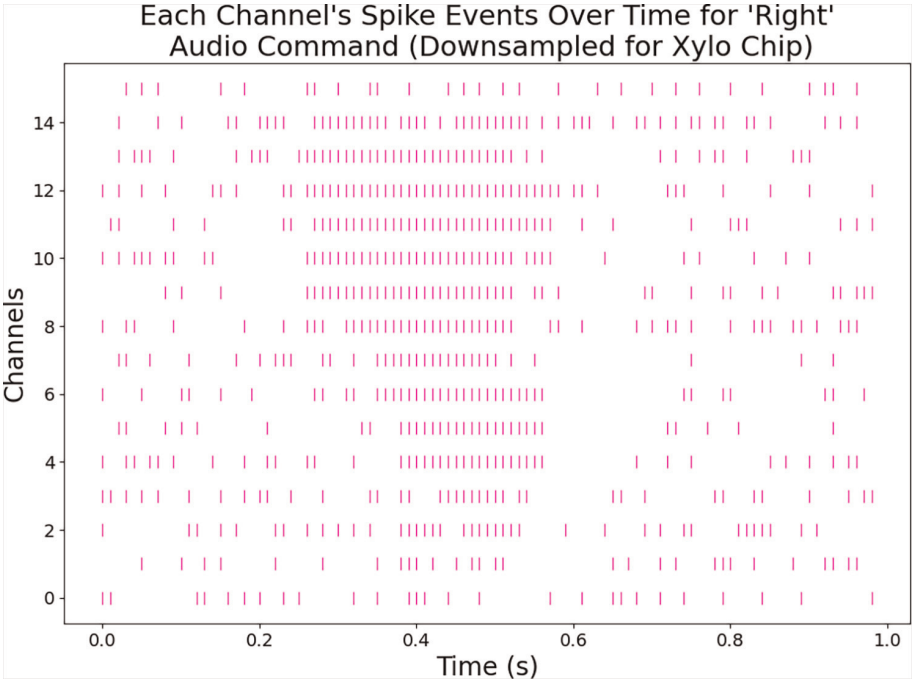

Figure 4.
Spike events for a down-sampled right audio command data.

Component	Power consumption (mW)
IO circuitry	213.94
Logic AFE	17.96
IO AFE	230.98
Logic	1844.26

Table 1.
Power consumption of Xylo neuromorphic chip.

consumption of only 17.96 mW, which provides reassurance about the chip's performance. These metrics underscore the feasibility and operational efficiency of implementing the associative learning system on the Xylo neuromorphic chip.

4. Simulations and experiments for associative learning in a T-maze using neuromorphic robot

In our system, detecting the red color is an unconditioned stimulus, while the audio command is a conditioned stimulus. When the robot detects the red color ahead, it stops and reverses direction, mimicking a rat's fear response. **Figure 5** depicts the experimental setup with our neuromorphic robot, and **Figure 6** illustrates the T-maze simulation and experimental scenarios. We developed specialized neuron models that convert audio commands and color data into spike signals to enable the robot to replicate a fear-conditioned response. Additionally, specific motion neurons are designed to control the robot's movements. These neurons are adaptations of the classic leaky integrate-and-fire (LIF) neurons, defined by the following equation:

$$C_m \frac{dV_m}{dt} = \frac{C_m}{\tau_{RC}}(E_L - V_m) + A \times I_{app}, \tag{1}$$

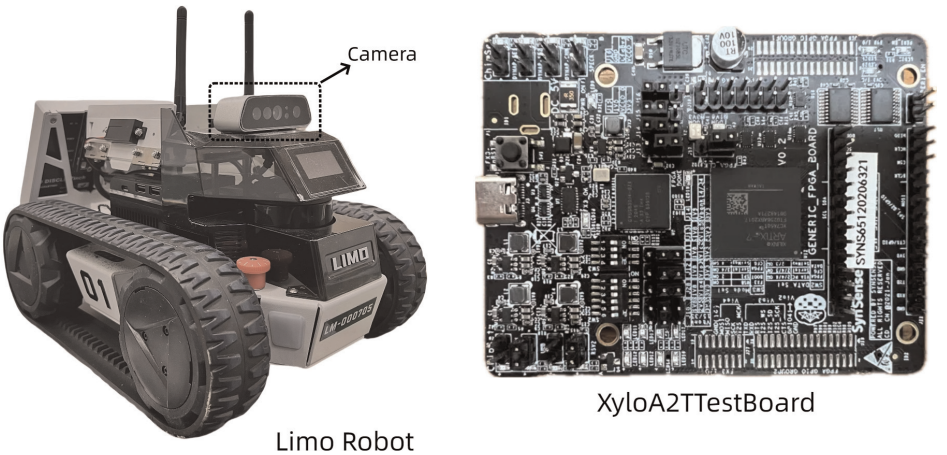

Figure 5.
Experimental setup of a mobile robot and Xylo neuromorphic chip.

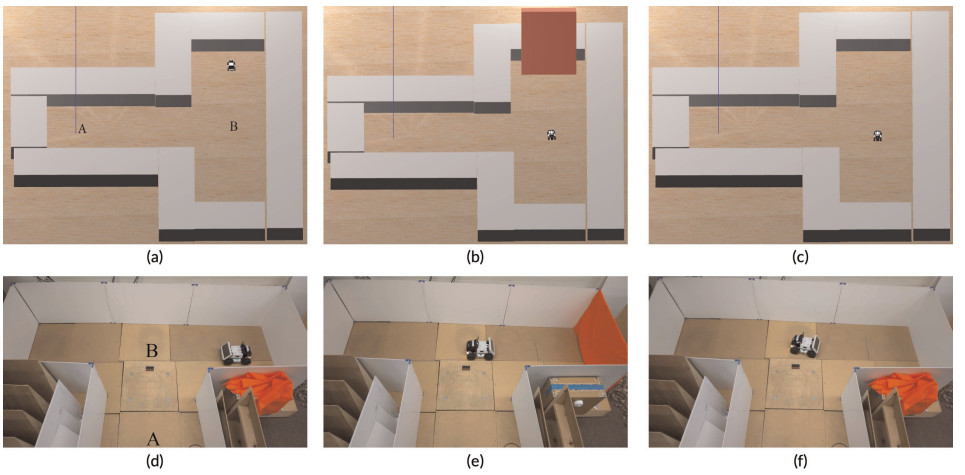

Figure 6.
Replicating Associative Learning in a T-Maze: Simulation and Experimental Exploration with a Neuromorphic Robot. (a) Gazebo simulation depicting the T-maze for robot navigation. (b) Detection of red color (US) input at position B. (c) The robot will learn to stop and turn to the arm with no red color presented. (d) The actual experimental setup of T-maze. (e) Detection of red color (US) input at position B in actual T-maze. (f) The robot will learn to stop and turn to the arm with no red color presented.

Neuron parameters	τ_{RC}	τ_{ref}	$V_{reset}(V)$	$V_{th}(V)$	Gain (A)
Color neuron	0.02	0.002	0.5	1.0	1.5
Command neuron	0.03	0.02	−0.5	0.9	1
Movement neuron	0.04	0.002	−0.1	0.8	1

Table 2.
LIF neuron parameters.

Where A denotes the input signal gain, is the membrane RC time constant, defines the membrane capacitance, and is the membrane potential leak potential (**Table 2**).

Table 2 lists the parameter values of the LIF neurons, which have been computed and refined to ensure they produce the desired experimental results. The gain and bias of the color-detecting neuron were determined empirically, ensuring it fires when detecting red stimuli but remains inactive for other colors.

The command neuron and LIF neurons calculate their gains and bias experimentally. The command neuron fires only when the aggregate output from the audio feature neurons is sufficiently high. The movement neuron fires whenever it receives continuous input spikes from the command or color neurons. The firing activations of these neurons are shown in **Figures 7–10**, respectively.

The XyloMonitor deployment tool facilitated real-time robot navigation via audio commands. This tool processes live audio inputs specifically in the “left” and “right” directions and predicts the robot’s intended direction. The XyloMonitor is configured to capture and process audio commands, with a brief waiting period mandated for the analog front-end (AFE) autocalibration, ensuring optimal and consistent audio data acquisition.

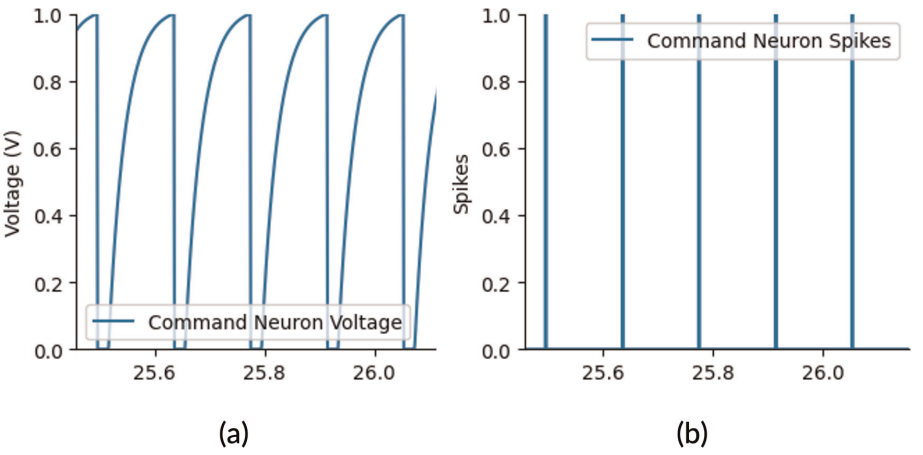

Figure 7.
Command neuron firing activity. (a) Membrane potential of command neuron (b) spiking activity of command neuron.

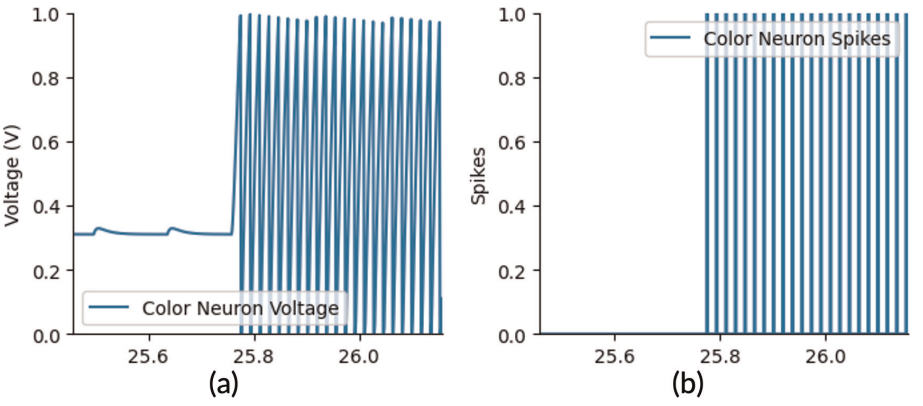

Figure 8.
Color neuron firing activity. (a) Membrane potential of color neuron (b) spiking activity of color neuron.

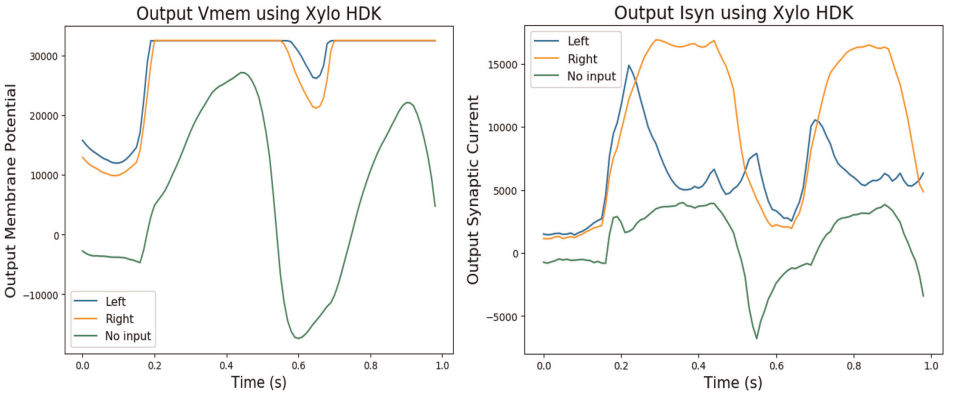

Figure 9.
Output membrane potentials and neuromorphic Xylo chip synaptic currents.

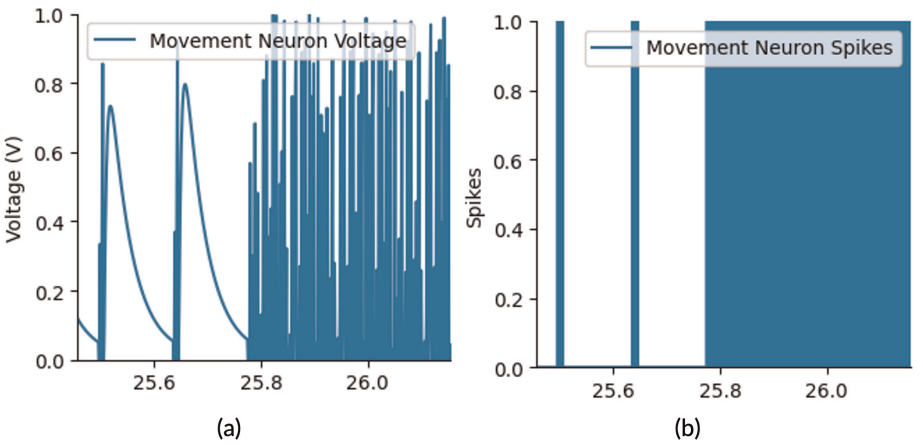

Figure 10.
Movement neuron firing activity. (a) Membrane potential of movement neuron (b) spiking activity of movement neuron.

Hebbian learning is utilized to adjust synaptic weights based on the principle that simultaneous activation of pre- and postsynaptic neurons strengthens their connection. The equation governing synaptic weight changes describes this adjustment. To manage variations in command delivery, such as differing volumes or distances from the microphone, the sensitivity of the audio capture system is increased using XyloMonitor, ensuring clear and accurate command recognition.

The Xylo neuromorphic chip processes incoming audio signals within a 250-millisecond time frame. The neuron's membrane potential, which indicates the received audio signal, determines the intended direction. If the membrane potential suggests "left," the robot turns left; if it suggests "right," the robot turns right. After processing, the determined direction is conveyed to the robot, directing its movement.

Figure 9 presents the membrane potential of audio neurons and the resulting synaptic currents on the Xylo neuromorphic chip in response to left and right audio commands.

Upon receiving a "left" or "right" command prediction from the Xylo neuromorphic chip, an additional neural network is deployed to control the robot's movement in the specified direction. This network includes ten LIF neurons specifically designed to ensure the robot steers accurately left or right.

The LIF neuron model is characterized by two key parameters: the membrane time constant and the refractory period. The refractory period is minimized to allow for rapid neuron firing following an output spike, enhancing the responsiveness of the robot's movements. Synaptic weights of the neurons are shown in **Table 3**.

The network receives a constant input, which generates a specific firing pattern when processed through the neurons with assigned synaptic weights. This pattern results in a mean firing probability, crucial for determining the robot's movement direction within the decision-making process. If the firing probability surpasses a threshold of 0.5, the neuromorphic robot turns left; if it falls below this threshold, then it turns right.

Specific synaptic weights and neuron properties are fixed to ensure the neuromorphic robot consistently turns left with a mean firing probability of 0.9. The following figure illustrates the firing probability of LIF neurons over time for the left turn. Neuron property are shown in **Table 4**.

Neuron index	Synaptic weights from input to neurons	Synaptic weights from neurons to output
1	45.0	9.0
2	−27.0	−18.0
3	72.0	27.0
4	−9.0	−36.0
5	63.0	45.0
6	−54.0	54.0
7	18.0	−63.0
8	81.0	72.0
9	−63.0	−81.0
10	9.0	9.0

Table 3.
Synaptic weights of the neurons for a left turn.

Parameter	Value
Membrane time constant	0.02
Refractory period	0.001
Seed	42

Table 4.
Neuron property for left turn.

Specific synaptic weights and neuron properties are established to guarantee that the neuromorphic robot consistently turns right with a mean firing probability of 0.2. **Table 5** illustrates the firing probability of LIF neurons over time for the right turn.

Neuron index	Synaptic weights from input to neurons	Synaptic weights from neurons to output
1	2.9	0.9
2	−0.5	−0.4
3	3.7	0.8
4	−0.3	−0.6
5	3.0	0.7
6	−0.6	0.8
7	0.8	−0.9
8	3.8	0.7
9	−0.7	−1.1
10	2.8	0.6

Table 5.
Synaptic weights of right-turning neurons.

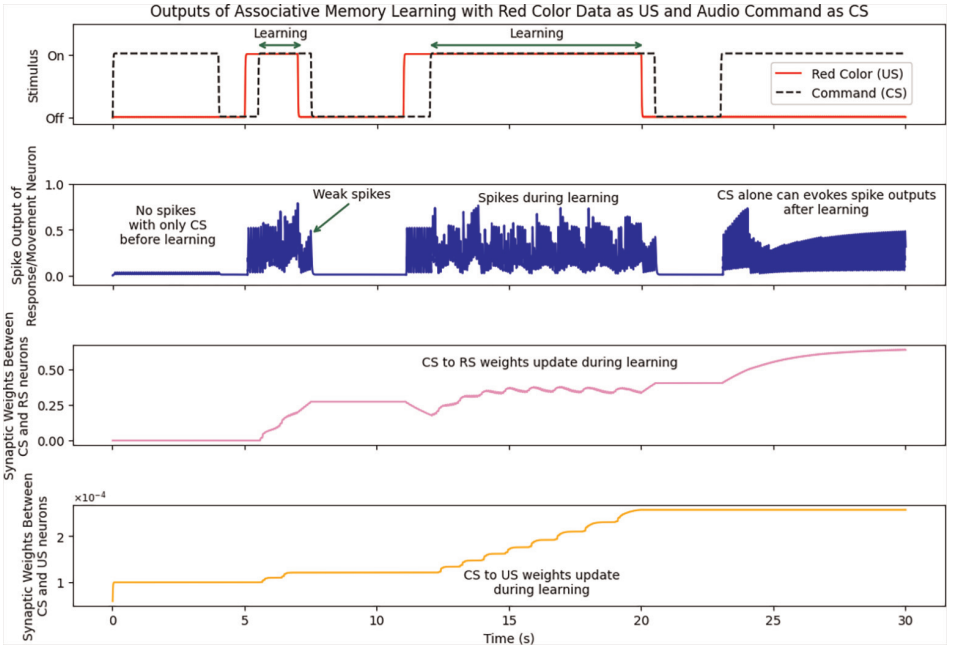

Figure 11.
Results of our associative learning.

The system's performance hinges on the pre- and postsynaptic neurons' learning and firing rates. In our experiment, the learning rate is set at 1e-4. **Figure 11** showcases the outcomes of our associative learning process.

Initially, the movement and audio command neurons (CS) possess low synaptic weights, preventing the movement neuron from responding to "left" and "right" auditory commands, resulting in no turns within the T-maze. Over time, associative learning updates the synaptic weights between the movement and audio command neurons. As a result, the movement neuron fires when the color-detection neuron detects red (US) through the camera. The activation of both command detection and movement neurons in response to combined color and audio stimuli strengthens the synaptic weights in the conditional signal pathway. **Figure 11** shows that the simultaneous application of red color and audio command stimuli enhances synaptic weights, though initially limited overlap leads to only moderate increases.

Insufficient overlap during the initial phase means that audio commands alone cannot trigger the movement neuron, as illustrated in **Figure 11**. However, with a more extended overlap period in the subsequent phase, there is a more significant increase in synaptic weights. Consequently, even without the red color input, the movement neuron will respond to auditory stimuli ("left" or "right" commands), demonstrating successful associative learning.

We replicated rat's associative learning experiments using a T-maze to evaluate and validate our associative learning system. **Figure 6** depicts both the simulation and experimental setups of our T-maze. In these setups, the red color functions as an unconditioned stimulus, while the audio commands act as conditioned stimuli.

Initially, the robot starts moving forward from the starting chamber, designated as position A and proceeds to the turning point, marked as position B. Upon reaching

position B, the robot receives a "left" or "right" command and turns 90 degrees accordingly, moving into the corresponding arm of the T-maze, as shown in **Figure 6(a)**.

In our simulation, the red color is assigned as an aversive stimulus. The robot responds to this unpleasant stimulus by turning away from the red color and heading toward the arm without the red color.

During associative learning, the robot initially moves from position A to B, encountering simultaneous turning commands and red color stimuli. The color-detection neuron fires in response to red, prompting the robot to choose the arm without the red color, as depicted in **Figure 6(b)**. During this phase, synaptic weights between the audio signal and movement neurons increase due to the concurrent audio and color spikes.

After 2–3 trials, the neuromorphic robot strengthens the synaptic connections related to the red color and audio commands, effectively memorizing the association. Consequently, even without the red color, the robot will move toward the "safe" arm it memorized—the arm without the red stimulus. **Figure 6(c)** shows that when the robot reaches position B, it stops, reverses 180 degrees to the right, and proceeds into the arm it has learned to identify as "safe". The real-world T-maze experiments mirror this associative learning process, as **Figure 6(d–f)** illustrates.

$$\Delta w = \eta\left(xy - \beta w y^2\right), \tag{2}$$

Where η is the learning rate, x is the firing rate of the presynaptic neuron, y is the firing rate of the postsynaptic neuron, β is a constant that determines the strength of the normalization, and w is the current synaptic weight.

Parameter	Value
Membrane time constant	0.02
Refractory period	0.002
Seed	42

Table 6.
Neuron property for right turn.

	Neuron	Task	Learning methods	Validation
[12]	6	N/A	N/A	Simulation
[13]	3	N/A	N/A	Simulation
[14]	5	N/A	N/A	Simulation
[11]	3	N/A	N/A	Simulation
[16]	3	N/A	N/A	Simulation
[17]	3	N/A	N/A	Simulation
[9]	20	N/A	Pretraining	Simulation
[18, 19]	1419	Fear conditioning	No pretraining	Experiment
This work	259	Spatial learning and memory	Self-learning	Simulation & Experiment

Table 7.
Synaptic weights of right-turning neurons.

The term serves as a mechanism to prevent weights from growing without bounds. It functions as a subtractive normalization, adjusting the scale of weight changes based on the weight's size and the postsynaptic activity. This approach helps maintain stability and control in learning, ensuring synaptic weights do not undergo uncontrolled growth. **Table 6** shows the results of the associative memory learning result. Then we make the comparison of scale and association capability with other works in **Table 7**.

5. Conclusion

This study presents the implementation of rodent-like associative learning in a T-maze using neuromorphic robots. By integrating the Xylo neuromorphic chip into a mobile robot, our system replicates the classic T-maze experiments observed in rodents. The robot learns to associate the red color (unconditioned stimulus) with audio commands (conditioned stimulus) through Hebbian learning and LIF neurons. Our findings demonstrate real-time associative learning, highlighting potential applications for autonomous robots operating in energy-constrained and adaptive environments.

Acknowledgements

This work was supported by the Robust Intelligence program in the Directorate for Computer and Information Science and Engineering (CISE) of National Science Foundation under Award Number 2245712.

Author details

Md Abu Bakr Siddique[1], Tianze Liu[1], Yan Zhang[2] and Hongyu An[1*]

1 Department of Electrical and Computer Engineering, Michigan Technological University, Houghton, MI, USA

2 Department of Biological Sciences, Michigan Technological University, Houghton, MI, USA

*Address all correspondence to: hongyua@mtu.edu

References

[1] Goodfellow I, Bengio Y, Courville A. Deep Learning. Cambridge, MA: MIT Press; 2016. Available from: http://www.deeplearningbook.org

[2] Devlin J, et al. Bert: Pre-training of deep bidirectional transformers for language understanding. arXiv preprint arXiv:1810.04805. 2018

[3] Sun C et al. Revisiting unreasonable effectiveness of data in deep learning era. In: Proceedings of the IEEE International Conference on Computer Vision. New York City, U.S.: IEEE; 2017

[4] Sengupta S et al. A review of deep learning with special emphasis on architectures, applications and recent trends. Knowledge-Based Systems. 2020; **194**:105596

[5] An H et al. Robust deep reservoir computing through reliable memristor with improved heat dissipation capability. IEEE Transactions on Computer-Aided Design of Integrated Circuits and Systems. 2020;**40**(3): 574-583

[6] Kandel ER, Schwartz JH, Jessell TM, Siegelbaum S, Hudspeth AJ, Mack S. Principles of Neural Science. Vol. 4. New York: McGraw-Hill; 2000

[7] Sun J et al. Memristor-based neural network circuit of full-function pavlov associative memory with time delay and variable learning rate. IEEE Transactions on Cybernetics. 2019;**50**(7):2935-2945

[8] Kohonen T. Self-Organization and Associative Memory. Vol. 8. New York, NY, USA: Springer Science & Business Media; 2012

[9] An H, An Q, Yi Y. Realizing behavior level associative memory learning through three-dimensional memristor-based neuromorphic circuits. IEEE Transactions on Emerging Topics in Computational Intelligence. 2019;**5**(4): 668-678

[10] Hu SG et al. Associative memory realized by a reconfigurable memristive Hopfield neural network. Nature Communications. 2015;**6**(1):7522

[11] Moon K et al. Hardware implementation of associative memory characteristics with analogue-type resistive-switching device. Nanotechnology. 2014;**25**(49):495204

[12] Yang J et al. A novel memristive Hopfield neural network with application in associative memory. Neurocomputing. 2017;**227**:142-148

[13] Liu X, Zeng Z, Wen S. Implementation of memristive neural network with full-function pavlov associative memory. IEEE Transactions on Circuits and Systems I: Regular Papers. 2016;**63**(9):1454-1463

[14] Hu X et al. Modeling affections with memristor-based associative memory neural networks. Neurocomputing. 2017; **223**:129-137

[15] Eryilmaz SB et al. Brain-like associative learning using a nanoscale non-volatile phase change synaptic device array. Frontiers in Neuroscience. 2014;**8**:205

[16] Ziegler M et al. An electronic version of Pavlov's dog. Advanced Functional Materials. 2012;**22**(13):2744-2749

[17] Pershin YV, Di Ventra M. Experimental demonstration of associative memory with memristive neural networks. Neural Networks. 2010;**23**(7):881-886

[18] Engelbrecht A, An H, Yi YC. Neuromorphic Computing. BoD–Books on Demand. Norderstedt, Germany; 2023

[19] Zins N, An H. Reproducing fear conditioning of rats with unmanned ground vehicles and neuromorphic systems. In: 2023 24th International Symposium on Quality Electronic Design (ISQED). New York City, U.S.: IEEE; 2023